Journal of Materials Chemistry C

ROYAL SOCIETY OF CHEMISTRY

PAPER

View Article Online
View Journal | View Issue

Cite this: *J. Mater. Chem. C*, 2021, **9**, 2321

Application of stimuli-responsive FRET behavior toward cyanide detection in a photo-switchable [2]pseudorotaxane polymer containing the BODIPY donor and the merocyanine acceptor†

Chinmayananda Gouda,[a] Debashis Barik,[a] Chandrima Maitra,[a] Kai-Chieh Liang,[a] Feng-Cheng Ho,[a] Venkatesan Srinivasadesikan,[b] Sarala Chandran,[b] Shu-Pao Wu,[b] Ming-Chang Lin[b] and Hong-Cheu Lin *[ac]

Received 21st October 2020,
Accepted 24th December 2020

DOI: 10.1039/d0tc05000h

rsc.li/materials-c

We have developed a supramolecular (close form) [2]pseudorotaxane polymer containing the green-emissive (λ_{em} = 523 nm) BODIPY-based pillar[5]arene host and the non-emissive spiropyran (SP)-based cyano guest (close form), which can be converted to a red-emissive (λ_{em} = 630 nm) merocyanine (MC)-based guest (open form) upon UV exposure as well as turned into a bi-fluorophoric host–guest polymer with ratiometric PL emission of Förster resonance energy transfer (FRET) behavior in THF/water solution (60% H_2O, v/v). The equal host–guest molar ratio and the formation of the [2]pseudorotaxane polymer can be further verified using ^{1}H NMR titration, Job's plot analysis, DOSY and ITC experiments. Hence, the bi-fluorophoric host–guest (with the MC open form) polymer possessed the highest red-emission of the MC acceptor, which was also confirmed using TRPL measurements to possess the shortest lifetime of 0.37 ns and the best FRET efficiency of 83.5%. Since the MC unit could react with CN^- to induce a non-emissive quenching process, the mono-fluorophoric guest would show turn-off PL behavior and detect cyanide ions with a corresponding limit of detection (LOD) value of 0.94 μM. In comparison, the optimal LOD value of 0.48 μM toward CN^- anion could be achieved by our bi-fluorophoric host–guest polymer *via* the FRET-OFF process. Therefore, cyanide detection and cell viability tests using the open form of the [2]pseudorotaxane polymer suggest useful bio-imaging applications in living cells.

Introduction

Cyanide (CN^-) is commonly known as a chemical warfare agent (CWA)[1–3] and is also a highly toxic species for living organisms. Being an extremely reactive substance, CN^- ions form a stable complex with cytochrome-*c* oxidase and inhibit the production of adenosine triphosphate (ATP) by interrupting the mitochondrial electron transport chain, which disrupts the central nervous system (CNS), resulting in cardiac arrest and death in humans.[4–6] According to the World Health Organization (WHO), the maximum permissible limit of cyanide in drinking water is 1.9 μM (70 ppb).[7] However, there is a huge demand for CN^- in various industrial applications, such as gold mining, electroplating, plastic manufacturing and metallurgy.[8] Due to its high toxicity and wide application range, the development of novel colorimetric[9] and fluorometric[10] chemosensors for cyanide detection based on the mechanisms of hydrogen-bonding interactions, nucleophilic addition, cyanide complexes and so on is highly demanded.[11,14] For example, some cyanide probes featuring turn-on and turn-off photoluminescence (PL) properties have been designed and developed to enhance the detection selectivity, sensitivity and reusability of these chemosensor materials.[12]

At present, some of the fluorometric sensor materials either fail to meet satisfactory accuracies or have poor detection capabilities toward the anionic analyte of CN^- due to the undesired interferences of PL signals by various factors, including poor solubility in water or semi-aqueous solutions, low selectivity to CN^-, a high detection limit and other surrounding stimuli (such as temperature, pH and light).[15] In general, most sensor probes towards various analyte detections were reported by either turn-on or turn-off fluorescence *via* mono-fluorophoric designs.[13] In order to overcome the shortcomings of poor sensitivity and a high limit of detection (LOD), a ratiometric fluorescence method

[a] *Department of Materials Science & Engineering, National Chiao Tung University, Hsinchu 300, Taiwan. E-mail: linhc@mail.nctu.edu.tw*
[b] *Department of Applied Chemistry, National Chiao Tung University, Hsinchu 300, Taiwan*
[c] *Center for Emergent Functional Matter Science, National Chiao Tung University, Hsinchu 300, Taiwan*

† Electronic supplementary information (ESI) available: UV-Vis and PL spectra, ^{1}H & ^{13}C NMR, elementary analysis, TRPL and HRMS (ESI) data. See DOI: 10.1039/d0tc05000h

via bi-fluorophoric design has been developed to achieve higher sensitivity in the PL measurements.[16] A FRET-based ratiometric method, which measures the ratio of fluorescence intensities at two wavelengths of the energy donor and acceptor, provides a unique approach to overcome the limitations of a single emission intensity of PL measurements. The Förster resonance energy transfer (FRET)[17] behavior is an efficient ratiometric approach in which an appropriate single excitation wavelength is required for an energy donor–acceptor bi-fluorophoric system, which results in a shorter emission lifetime of the energy donor and induces a higher PL contrast after the FRET process. Therefore, the enhanced ratiometric PL signals with improved LOD values obtained *via* the FRET process can be applied in highly sensitive chemosensing.

Since two chromophores are required in the energy donor–acceptor bi-fluorophoric system for the FRET process, the donor chromophore should have a shorter emission wavelength to overlap with the absorption of the acceptor chromophore to be utilized in the FRET sensor materials. Thus, efficient green emitters, such as boron-dipyrromethene (BODIPY) derivatives, can be chosen as donor chromophores for the FRET sensor materials. The BODIPY-based chromophores belong to a distinct class of fluorescent molecules, which have extensive applications in various fields, such as light-harvesting systems, laser dyes,[18] and photosensitizers.[19,20] Due to possessing the traditional aggregation caused quenching (ACQ)[21] behavior, BODIPY molecules can be used in bio-medical fields such as fluorescent biosensing[22] and deep tissue tumor imaging,[23] biochemistry,[24] and other related fields. Due to the conjugation of π-electrons, BODIPY molecules show long absorption wavelengths, which fall in the visible region. Moreover, because of the small Stokes shift, BODIPY derivatives lose a very low amount of energy through non-radiative decay *via* vibrational relaxation, which leads to their high quantum yield and excellent photostability, along with strong emissions in the visible region.

Interestingly, a class of stimuli-responsive photochromic spiropyran (SP) derivatives[25–27] can be used as effective energy acceptors and highly luminescent red chromophores for the FRET sensor materials, which produce distinct color changes *via* reversible isomerization from a closed form (SP) to a highly polar open-ring metastable merocyanine (MC) upon irradiation with UV light.[28] The ring-opening mechanism has been proven by a heterocyclic C–O bond cleavage to induce a longer π-conjugation length, which leads to a zwitterionic planar MC form. Moreover, the positive charge on nitrogen atom plays the pivotal role for MC to be an emerging probe toward the selective nucleophilic addition of cyanide ion.[29] Nonetheless, what makes SP unique among all photoswitchable probes[30] is that two isomers of SP and MC units are reversibly controlled by different external stimuli like pH, temperature, solvent,[31] mechanical force,[32,33] redox potential,[34] and different analytes, which demonstrate more flexible applications in optical switches,[35] data storage media,[36] functional materials,[37] and chemo-[38] and biosensors.[39] Since the MC unit in the open form behaves as an energy acceptor, it can also be used as a cyanide detection probe in a highly selective and sensitive manner.[40] Moreover, FRET-based ratiometric cyanide detection with appreciable sensitivity and bio-applicability in pure water using an amphiphilic copolymer containing covalently linked bifluorophoric MC and tetraphenylethylene (TPE) units and its aggregation induced emission (AIE) properties have been explored in our previous study.[41,42]

Supramolecular polymers are a type of polymer in which the monomers are connected by different kinds of non-covalent interactions (host–guest, hydrogen bonding, π–π stacking, metal–ligand, *etc.*).[43] Meanwhile, supramolecular polymers featuring dynamic non-covalent interactions exhibit many special properties, including reversible,[44] degradable,[45] self-healable,[46] and stimuli-responsive properties,[47] which can be utilized in biomaterials,[48] organic electronics,[49] drug delivery,[50] and smart materials.[51] Over the past few decades, a wide variety of macrocycles have been used as host molecules, such as crown ethers,[52] cucurbit[*n*]urils,[53] calix[*n*]arenes,[54] pillar[*n*]arenes (PAs),[55] and cyclodextrins[56] (CDs), to mix with equal molar amounts of complimentary guest components, such as secondary ammonium salts, paraquat, pyridinium, fullerenes, ferrocenium, tropylium, imidazolium, Lewis basic anions (*e.g.*, halides) and polyatomic molecules, azobenzene, 1,4-dicyanobutane and adamantine.[57] Since the first report on PAs by Ogoshi in 2008,[58] they have attracted extensive attention due to their distinct structural advantages as host molecules, such as electron-rich cavities, facile modifications and symmetrical rigid structures, which are different from those of resorcinarenes, calixarenes and cyclotriveratrylenes. Pillararenes consisting of substituted hydroquinone units linked by methylene bridges possess rigid and π-rich cavities, which are very suitable as potential receptors for cationic guests through hydrogen bond, cation–π–electron and ion–dipole interactions. Pillararenes also have good binding affinities toward cationic units (including viologens, bisimidazolium, ammonium and bispyridinium salts), anionic units (including 1-octanesulfonate and naphthalenesulfonates) and neutral motifs (linear *n*-alkanes, alkanediols, dicyanoalkanes, haloalkanes, azide compounds), which have been widely employed in host–guest supramolecular systems.[59,60] Due to their feasible synthesis and good binding affinities towards neutral guests, nitrile/cyano derivatives are suitable to be used as quest moieties for the host–guest complexation with pillararenes.[61]

Owing to the benefits of non-covalent interactions, including self-healing, stimuli-responsive properties and reversibility,[62–64] some novel host–guest sensor materials have garnered more attention than the traditional covalently linked bi-fluorophoric FRET chemosensors.[65] Therefore, supramolecular polymer FRET-based chemosensing probes (such as pseudorotaxane polymer) have been developed recently.[66] Herein, we introduce a photo-switchable, stimuli-responsive and bio-compatible supramolecular [2]pseudorotaxane polymer to carry out cyanide detection in semi-aqueous solutions. To achieve this supramolecular assembly, we designed and synthesized a host–guest FRET system as displayed in Scheme 1, which consists of a spiropyran-based ditopic guest (**SP-G**) containing two terminal cyano binding groups and a BODIPY-based ditopic host (**BP5-H**) containing two terminal pillar[5]arenes to obtain a 1 : 1 host–guest complex (**BP5-H⊃SP-G**).

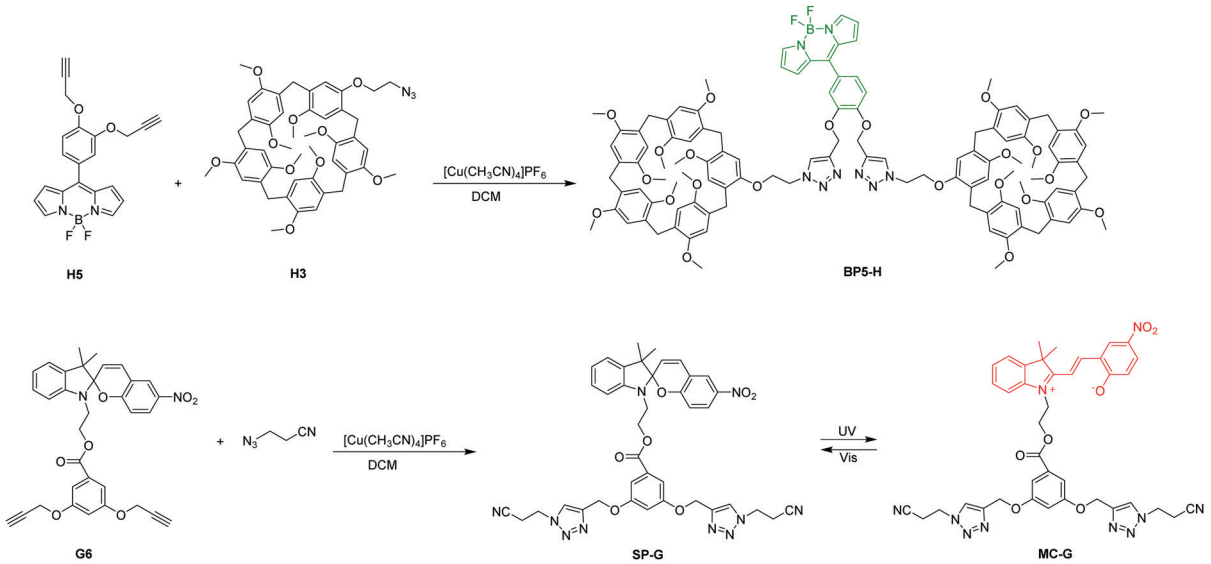

Scheme 1 Synthetic routes of (a) the host **BP5-H** and (b) the guest **SP-G**.

This host–guest mediated self-assembly satisfies the FRET condition of the BODIPY-donor and the spiropyran-acceptor upon UV exposure to produce the active FRET host–guest complex (**BP5-H⊃MC-G**), which reveals remarkable selectivity and sensitivity toward cyanide ion detection along with cell imaging tests *via* a FRET-OFF process.

Results and discussion

Design and synthesis of the supramolecular polymer

In order to develop a new approach for highly selective and sensitive detection of CN^- anion using chemosensors, we introduce a new supramolecular host–guest FRET-based assembly, the synthetic routes of which are illustrated in Scheme 1, which contains bifluorophoric boron-dipyrromethene (BODIPY) and spiropyran (SP) moieties as the green-emission energy donor and the red-emission energy acceptor, respectively. Herein, the supramolecular host–guest system, *i.e.*, **BP5-H⊃SP-G** (1 : 1), was constructed *via* the supramolecular interaction of the bis-pillar[5]arene host (**BP5-H**) and the di-cyano guest (**SP-G**), wherein the central BODIPY unit was attached to two macrocycles (*i.e.*, di-pillar[5]arene) to obtain the BODIPY-bridged bis-pillar[5]arene host **BP5-H** and the other central photochromic SP unit was linked *via* the click reaction of two cyano groups to produce the photoswitchable SP-bridged dicyano guest **SP-G**. Since the reversible isomerization from a closed form (SP) to a highly polar open-ring metastable merocyanine (MC) can be proceeded upon irradiation with UV light, the photoswitchable SP-bridged dicyano guest **SP-G** can be transformed to the other MC-bridged dicyano guest **MC-G** as shown in Scheme 1. Accordingly, the supramolecular host–guest system, *i.e.*, **BP5-H⊃MC-G** (1 : 1), was obtained from the previously prepared host–guest system **BP5-H⊃SP-G** upon UV exposure.

Hence, the overlap of the photoluminescence (PL) emission of the donor BODIPY unit (**BP5-H**) with the absorption of the acceptor MC unit (**MC-G**) in semi-aqueous solution after UV exposure is required for efficient energy transfer, but the supramolecular interaction to bring the energy donor and acceptor within adjacent distance in the host–guest system may warrant the FRET process, which can be further employed in the potential sensing applications of **BP5-H⊃MC-G**. Accordingly, this ratiometric FRET process can induce noticeable and enhanced synergistic dual emissions of host and guest fluorophores **BP5-H** and **MC-G**. Since the MC unit after UV exposure can be utilized to detect cyanide anion and applied for bioimaging tests in living cells, various FRET phenomena (depending on water content, UV exposure, pH and temperature) are investigated using UV-vis and PL spectroscopy, TRPL, DLS, XRD, as well as DFT computations in this study.

Confirmation of the host–guest interaction of the pseudo-rotaxane polymer

The host–guest interactions in the formation of the supramolecular assembly between **BP5-H** and **SP-G** were studied using ^{1}H NMR spectroscopy in a 1 : 1 $CDCl_3$–CD_3CN mixture. As shown in Fig. 1, the complexation between **SP-G** and **BP5-H** is a fast exchange process on the NMR time scale based on the proton signals of **BP5-H**, **SP-G** and a 1 : 1 equiv. host–guest mixture of **BP5-H** and **SP-G** (*i.e.*, **BP5-H⊃SP-G**). Similarly, the host–guest interactions of **BP5-H** and **MC-G** (*i.e.*, **BP5-H⊃MC-G**) after UV exposure were also confirmed for the formation of the supramolecular assembly using ^{1}H NMR spectra shown in Fig. S21 (ESI†).

Upon the addition of 1.0 equiv. of **SP-G** to **BP5-H** solution, the resonance for H_1, H_2 and H_3 of **SP-G** showed small upfield shifts due to the shielding effect of electron-rich cavity provided by the pillar[5]arene macrocycle. Besides, the H_a, H_b, H_c and H_d protons of **BP5-H** appeared in the small downfield region because of the deshielding effects on the protons exposed outside the electron-rich pillar[5]arene. There are also remarkable peak

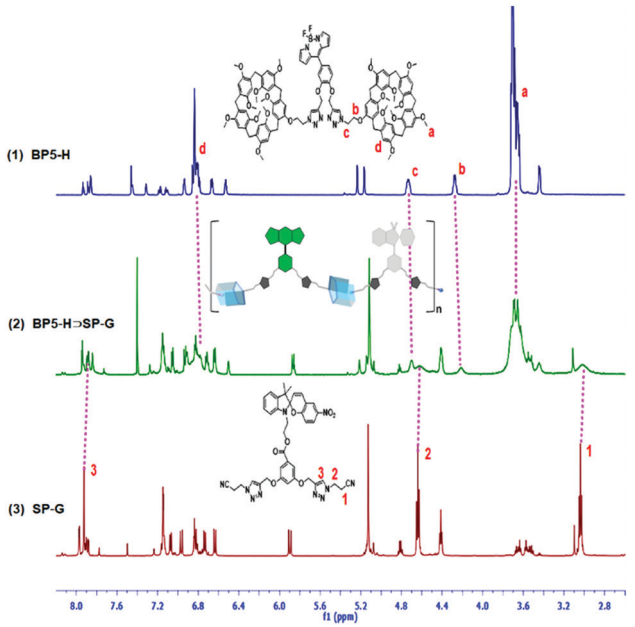

Fig. 1 ^{1}H NMR spectra (300 MHz, 1 : 1 $CDCl_3$–CD_3CN, 298 K) of (1) **BP5-H** (5.0 mM), (2) a 1 : 1 mixture of **BP5-H** and **SP-G** (5.0 mM each) and (3) **SP-G** (5.0 mM).

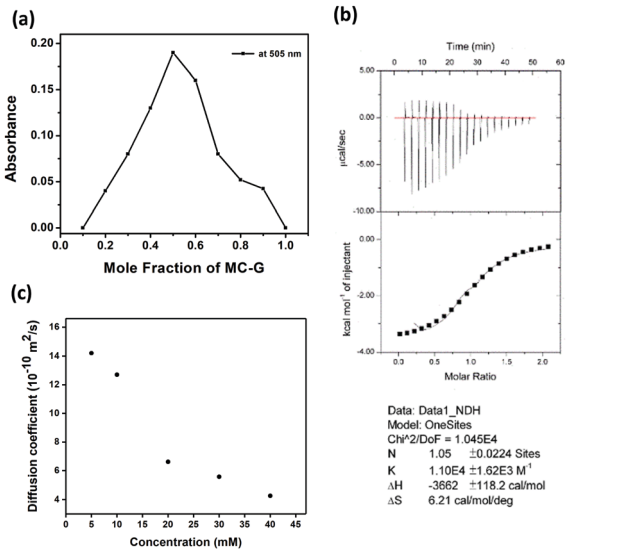

Fig. 2 (a) Job's plot of 1 : 1 stoichiometry between **BP5-H** and **MC-G** complexation by plotting the absorbance difference at 505 nm against the mole fraction of **MC-G** in a THF/H_2O mixture (60% H_2O, v/v). (b) Titration profiles at 298 K when **BP5-H** (2.0 mM) was mixed with **SP-G** (20.0 mM) in semi-aqueous solution (THF/water = 4 : 6 v/v) at 25 °C. The raw ITC data for sequential injections of 2 μL per injection of **SP-G** solution (20.0 mM) into **BP5-H** solution (2.0 mM) with at 4 s intervals between injection and net reaction were obtained by subtracting the dilution heat from the reaction heat, fitted by the "one set of binding site" model. The average data of repeated ITC experiments: K_s = (1.14 ± 0.10) × 10^{-4} M^{-1}, ΔH = −2.19 ± 0.97 kJ mol^{-1}, $T\Delta S$ = 33.38 ± 9.92 kJ mol^{-1}. (c) DOSY measurements (500 MHz, $CDCl_3/CD_3CN$ = 1 : 1, 298 K) of **BP5-H/SP-G** (1 : 1 molar ratio) at various concentrations (1–40 mM).

broadenings of the H_1, H_2 and H_3 protons of **SP-G** along with the H_a, H_b and H_d protons of **BP5-H** clearly indicating the existence of host–guest pseudorotaxane due to the interaction between the electron-deficient nitrile unit of **SP-G** and the electron-rich cavity of **BP5-H**. It is worth mentioning that some parts of proton signals for H_a, H_b, H_c and H_1, H_2 and H_3 are almost unchanged, which firmly demonstrate that both complexation and un-complexation between **SP-G** and **BP5-H** take place simultaneously. Moreover, another model host–guest system containing the pillar[5]arene macrocycle host (**M-H**) and the cyano guest (**M-G**) was synthesized as shown in Schemes S3 and S4 (ESI†),[67,68] in which their detailed synthetic procedures and chemical characterization (Fig. S22–S27) are shown. With the investigation of the model host–guest system (*i.e.*, **M-H**⊃**M-G**) explained in the ESI,† the host–guest interaction of pseudo-rotaxane is confirmed *via* NMR studies as illustrated in Fig. S28 (ESI†).

To support the NMR titration results, we investigated the binding mode between the host and guest molecules using Job's plot analysis (Fig. 2a), which also illustrates the 1 : 1 complexation between **BP5-H** and **MC-G**. Furthermore, to obtain details of the thermodynamics of host–guest complexation, we performed the isothermal titration calorimetry (ITC) measurements of **BP5-H** *vs.* **SP-G** (Fig. S2b, ESI†). The association constant obtained from the average data of repeated ITC experiments was in the range of (1.14 ± 0.10) × 10^{-4} M^{-1}, which demonstrates the strong binding affinity of the neutral cyano guest toward the **BP5-H** host. The association constant obtained from this titration was in the order of ∼10^4 M^{-1}, which demonstrates a strong binding affinity of the neutral cyano guest toward the **BP5-H** host. Additionally, two-dimensional diffusion-order NMR spectroscopy (diffusion ordered spectroscopy, DOSY) was also performed to investigate the self-assembly behavior of **BP5-H**⊃**SP-G** between **BP5-H** and **SP-G** (1 : 1) (Fig. 2c). The values of the weight average diffusion coefficient decrease notably from 14.2 × 10^{-10} to 4.23 × 10^{-10} m^2 s^{-1} during the addition of **BP5-H** from 5 to 40 mM, as **SP-G** is fixed at 40 mM. The findings from these data clearly revealed the formation of the supramolecular polymeric cluster by virtue of the host–guest interaction.

AIE behavior at various water fractions

To explore the aggregation caused quenching (ACQ) and aggregation-induced emission (AIE) properties of both fluorophores **BP5-H** and **MC-G**, respectively, the photophysical studies of the individual host and guest were carried out in THF/water solution (with different water contents). **BP5-H** and **MC-G** showed absorbance at 490 nm and 550 nm (Fig. S29 and S30, ESI†), respectively, in 60% H_2O/THF. In pure THF, **BP5-H** showed strong green PL emission at 527 nm. The intensity gradually decreased upon subsequent addition of water in the THF solution. As the water content reached 60%, the PL intensity reduced to one-third of its initial intensity (Fig. 3a and b) due to the ACQ effect. Notably, the fluorescence behavior of the guest **MC-G** exhibited a completely reverse phenomenon to that of the host **BP5-H** in THF/water solution. Initially, there was no emission of the guest **MC-G** in pure THF. The emission at 630 nm gradually increased with an increase in water percentage and reached the maximum emission

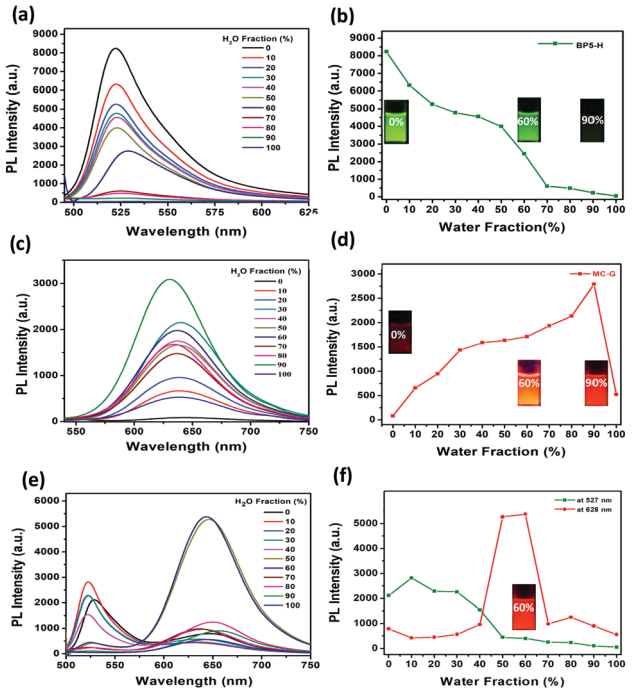

Fig. 3 PL spectra of (a) **BP5-H** (63 μM) and (c) **MC-G** (63 μM) under UV exposure with increasing water fraction from 0% to 100% in THF/water solution at excitation wavelengths of 490 and 540 nm, respectively. (e) **BP5-H⊃MC-G** (1 : 1) (63 μM) under UV exposure with increasing water fraction from 0% to 100% in THF/water solution at an excitation wavelength of 490 nm. Plot of the maximum PL emission intensities of (b) **BP5-H**, (d) **SP-G** and (f) **BP5-H⊃MC-G** (1 : 1) *vs.* water fraction in THF/water (60% H_2O, v/v) solution (63 μM). Insets: Fluorescence images of (b) **BP5-H**, (d) **MC-G** and (f) **BP5-H⊃MC-G** (1 : 1) in THF/water (0, 60, 90% H_2O, v/v) solution (63 μM) upon UV exposure (λ_{ex} = 365 nm).

at a 90% water fraction. Then, a sudden drop in the PL intensity of **MC-G** was observed at a 100% water content, and the bright red emission was diminished consequently (Fig. 3c and d).

Because of the photoisomerization of the SP unit, the close non-emissive form of **SP-G** was gradually transformed into the emissive **MC-G** form upon UV irradiation and then we studied the extent of photoisomerization with respect to different UV exposure times (Fig. S31, ESI†). The maximum emission was obtained from MC-G after 120 s of UV exposure and hence we chose this exposure time throughout our experiment. The reversibility of both the forms under alternative UV and visible light exposure was checked up to five consecutive cycles without any substantial deviations (Fig. S32, ESI†).

The opposite ACQ and AIE behaviors of the PL properties of **BP5-H** and **MC-G**, respectively, tended us to investigate the aggregation effects of these two fluorophores in the host–guest system; hence, we carried out PL studies for **BP5-H⊃MC-G** (1 : 1) in THF/water solutions with different water contents (Fig. 3e). The green PL emission intensity at 527 nm and the red PL emission intensity at 630 nm are plotted in Fig. 3f. The PL intensity of the host–guest system **BP5-H⊃MC-G** was initially reduced due to the ACQ behavior of **BP5-H**. Then, a dramatic enhancement and optimal PL emissions of **BP5-H⊃MC-G** at 630 nm were obtained at a water content of *ca.* 50–60% due to the FRET behavior from **BP5-H** to **MC-G** units, which was confirmed by the overlap of the photoluminescence (PL) emission of the donor BODIPY unit (**BP5-H**) with the absorption of the acceptor MC unit (**MC-G**) for efficient energy transfer (Fig. S33, ESI†). The 1 : 1 host–guest **BP5-H⊃MC-G** showed the optimal PL emission at a water content of *ca.* 60% from the contribution of the AIE emission of **SP-G** and the reasonable ACQ emission from **BP5-H**, but the FRET emission of the host–guest **BP5-H⊃MC-G** at 630 nm could not be further enhanced because the optimal AIE emission of **SP-G** at a 90% water content could not be matched with the energy donor of PL emission from **BP5-H**, where the serious ACQ of **BP5-H** occurred. Therefore, the best energy transfer from the donor **BP5-H** to the acceptor **MC-G** with the highest PL emission of the host–guest **BP5-H⊃MC-G** (1 : 1) at 630 nm at a 60% water content was chosen for our study in further experiments.

Due to the efficient FRET behavior from the energy donor **BP5-H** to the acceptor **MC-G**, the highest PL emission at 630 nm was observed in the host–guest **BP5-H⊃MC-G** (1 : 1) in semi-aqueous media with a 60% water content as shown in Fig. 3f, and the PL properties of **BP5-H/MC-G** (1 equiv./0.0–1.4 equiv.) mixtures with different equivalents of **MC-G** in THF/water solution (60% H_2O, v/v) are displayed in Fig. 4a, where the PL emissions of **BP5-H** and **MC-G** at 527 and 630 nm were investigated, respectively. This revealed that the maximum green PL emission intensity of the donor **BP5-H** (1 equiv.) at 527 nm decreased gradually upon the addition of the guest **MC-G** (0.0–1.4 equiv.). However, the maximum red PL emission intensity of the guest **MC-G** at 630 nm increased almost linearly and reached the highest intensity at a host–guest stoichiometry of 1 : 1. Hence, the saturated red PL emissions of **BP5-H/MC-G** (1 equiv./1.1–1.4 equiv.) mixtures were observed with over-supplied equivalents of the guest **MC-G** (1.1–1.4 equiv.). In addition, the fluorescence images of green-emissive **BP5-H** (63 μM) and red-emissive **BP5-H/MC-G** (1 : 1, *i.e.*, **BP5-H⊃MC-G**) in THF/water solution (60% H_2O, v/v) under UV light (λ_{ex} = 365 nm) are also demonstrated in the insets of Fig. 4b. Moreover, this result suggested the 1 : 1 complexation ratio between **BP5-H** and **MC-G**,

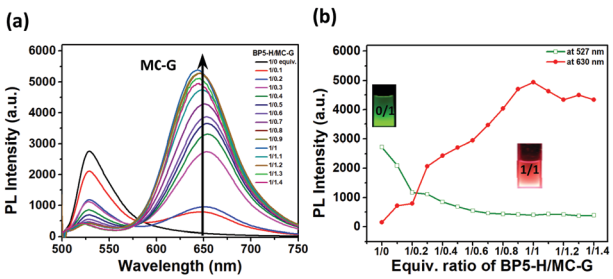

Fig. 4 (a) PL spectra and (b) relative PL intensities of **BP5-H/MC-G** (1 equiv./0.0–1.4 equiv.) at 527 nm and 630 nm under UV exposure with the gradual addition of **MC-G** (0.1 equiv., 63 μM) up to 1.4 equiv. into **BP5-H** (1 equiv., 63 μM) in THF/water solution (60% H_2O, v/v) at an excitation wavelength of λ_{ex} = 490 nm. Insets: Fluorescence images of **BP5-H** and **BP5-H/MC-G** (1 : 1, *i.e.*, **BP5-H⊃MC-G**) in THF/water (60% H_2O, v/v) solution (63 μM) upon UV exposure (λ_{ex} = 365 nm).

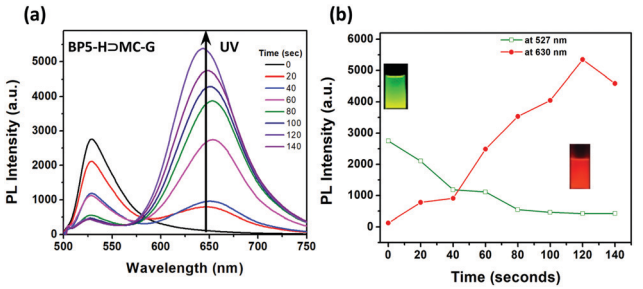

Fig. 5 Time-dependent (a) fluorescence spectra and (b) maximum PL intensities of both green donor and red acceptor emissions of **BP5-H⊃MC-G** (63 μM) in THF/water solution (60% H_2O, v/v) at an excitation wavelength of λ_{ex} = 490 nm. Insets: Photos of PL color changes before and after UV exposure (λ_{ex} = 365 nm).

which was also supported by the results of ^{1}H NMR titration, Job's plot analysis and ITC experiments. Furthermore, we calculated the FRET efficiency by using the equation shown in Fig. S34 (ESI†), which showed a remarkable FRET efficiency of 83.5%.

To explore the suitable UV exposure time for **BP5-H⊃MC-G**, we studied different time intervals of UV exposure, as shown in Fig. 5a. This revealed that the maximum FRET emission of **BP5-H⊃MC-G** was observed after 120 s of UV exposure, and then there is a small reduction in the red emission after 140 s of UV exposure. Hence, we concluded 120 s as the best UV exposure time for all the experiments in this study.

Effects of pH on the FRET process of the host–guest BP5-H⊃MC-G

Since the guest **SP-G** has no PL emission without UV exposure, only the host–guest **BP5-H⊃MC-G** (1 : 1) and the guest **MC-G** were treated at different pH values after UV exposure to observe the effects of pH on the FRET processes between the green emission of the energy donor **BP5-H** and the red emission of the energy acceptor **MC-G.** As illustrated in Fig. 6b, the host–guest **BP5-H⊃MC-G** (1 : 1) in THF/water solution (60% H_2O, v/v) upon UV exposure (λ_{ex} = 365 nm) showed a strong red PL emission at pH = 7 with the occurrence of an efficient FRET process between the energy donor **BP5-H** and the acceptor **MC-G** initially; hence, the host–guest **BP5-H⊃MC-G** showed strong red PL emissions under neutral conditions (*i.e.*, pH = 5–9). At lower pH values (*i.e.*, pH = 1–3), the PL emission color of **BP5-H⊃MC-G** was slightly orange. On the contrary, the green PL emission color (FRET OFF) of **BP5-H⊃MC-G** was achieved at higher pH values (*i.e.*, pH = 11–13) due to the closed form of **SP-G.** As a comparison, the acceptor **MC-G** also shows various PL emission intensities at different pH values as shown in Fig. S35 (ESI†), which showed similar trends of strong red PL emission at pH = 7 that is almost quenched at low pH values of 1–2 and high pH values of 11–13 (to transform into the closed form of **SP-G**).[5] Hence, we can conclude that the efficient FRET process of the host–guest **BP5-H⊃MC-G** can only occur at neutral pH values (*i.e.*, pH = 5–9) as the energy donor **BP5-H** transferred the energy to the open form of the energy acceptor **MC-G.**

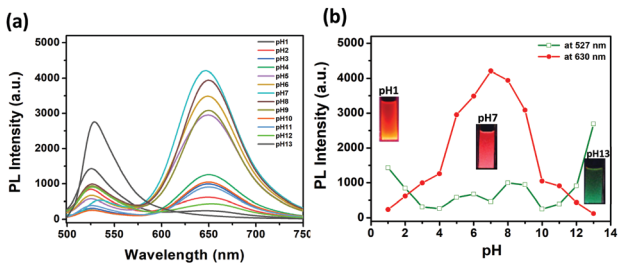

Fig. 6 (a) PL spectra and (b) relative PL intensities of **BP5-H⊃MC-G** (1 : 1) (63 μM) at 527 nm and 630 nm upon UV exposure (365 nm) at different pH values in THF/water solution (60% H_2O, v/v) at an excitation wavelength of λ_{ex} = 490 nm. Insets: Fluorescence images of **BP5-H⊃MC-G** and **MC-G** at different pH values (pH = 1, 7 and 13) after UV exposure (λ_{ex} = 365 nm).

Effects of temperature on the FRET process of the supramolecular polymer

As we know, the isomerization of SP from the open to the closed form can be observed by increasing the temperature up to 60 °C. Hence, the effects of temperature on the FRET process of the host–guest **BP5-H⊃MC-G** (1 : 1) in THF/water solution (60% H_2O, v/v) upon UV exposure (λ_{ex} = 365 nm) were also examined over the temperature range from 10 °C to 60 °C and are shown in Fig. 7. At lower temperatures (10–45 °C), the PL emission colors of **BP5-H⊃MC-G** were slightly orange. However, when the temperature exceeded 50 °C (up to 60 °C), the green PL emission color (FRET OFF) of **BP5-H⊃MC-G** was achieved due to the closed form of **SP-G.** Therefore, the FRET processes from the donor **BP5-H** to the acceptor **MC-G** can be adjusted in the temperature range of 10 °C to 40 °C and the temperature above 45 °C is not applicable for the FRET process.

Cyanide sensing of the supramolecular polymer

Since CN^- anion as a strong nucleophile group can attack electron deficient groups, such as the indolium (–C–C=N^+) group,[5–10,15] *via* nucleophilic addition, the carbon atom of (–C=N^+) in the MC unit could react with CN^- to induce a non-emissive MC–CN structure, resulting in the interruption of MC π-conjugation[10] to shut down the red MC emission in the guest **MC-G** or to turn off the ratiometric emission of the FRET

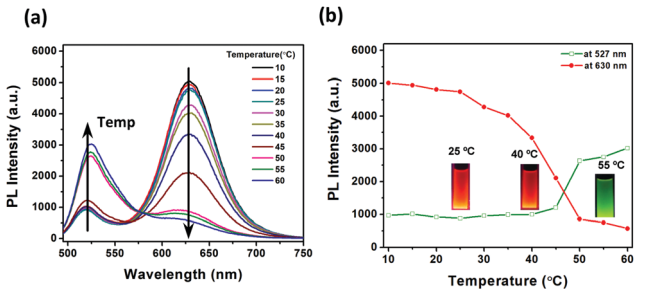

Fig. 7 (a) PL spectra and (b) relative PL intensities of **BP5-H⊃MC-G** (1 : 1) (63 μM) at 527 nm and 630 nm (after UV exposure) upon heating at different temperatures in THF/water solution (60% H_2O, v/v) at an excitation wavelength of λ_{ex} = 490 nm. Insets: Fluorescence images of **BP5-H⊃MC-G** and **MC-G** at different temperatures (15, 30 and 55 °C) after UV exposure (λ_{ex} = 365 nm).

process. As described previously, the closed form of the photochromic spiropyran (SP) unit in the guest **SP-G** can be transformed into the open form of the merocyanine (MC) unit in the guest **MC-G** after UV irradiation. Therefore, both the mono-fluorophoric guest **MC-G** and the bi-fluorophoric host–guest **BP5-H⊃MC-G** can react with CN^- anion to enable cyanide sensing. Herein, we performed PL titration experiments of the bi-fluorophoric host–guest **BP5-H⊃MC-G** in THF/water solution (60% H_2O, v/v) upon the addition of different concentrations (0–60 μM) of CN^- anion to demonstrate the FRET-OFF processes in the ratiometric PL changes at two relevant wavelengths of green BODIPY emission at 527 and red MC emission at 630 nm as shown in Fig. 8a. As the concentration of CN^- anion increased, as shown in Fig. 8a, the red-emission of the MC unit at 630 nm became weaker, and the green emission of the BODIPY unit at 527 nm became stronger in the host–guest **BP5-H⊃MC-G**. The ratiometric PL ratio (I_{630}/I_{527}) of the bi-fluorophoric host–guest **BP5-H⊃MC-G** titrated with different concentrations (0–50 μM) of CN^- anion and the relative PL ratio (I/I_0) of the mono-fluorophoric guest **MC-G** titrated with different concentrations (0–90 μM) of CN^- anion are displayed in Fig. 8a and b, respectively. As illustrated in Fig. 8c, the best limit of detection (LOD) toward analyte CN^- anion was 0.48 μM, which was achieved by our host–guest **BP5-H⊃MC-G,** and the LOD value obtained by the guest **MC-G** was 0.94 μM as shown in Fig. 8d. Furthermore, the LODs of **BP5-H⊃MC-G** and **MC-G** are much lower than the maximum permissible limit of cyanide in drinking water (*i.e.*, 1.9 μM (70 ppb) set by the WHO).[7] Moreover, we also examined the sensing selectivity of our probes, the bi-fluorophoric host–guest **BP5-H⊃MC-G** and the mono-fluorophoric guest **MC-G,** by titrating with various analytes (100 μM), including Cl^-, F^-, Br^-, I^-, AcO^-, HCO_3^-, CO_3^{2-}, CN^-, NO_2^-, NO_3^-, PF_6^-, SO_4^{2-}, $H_2PO_4^-$, HPO_4^{2-}, L-Cys, ClO_2^- and GSH, in THF/water solution with a 60% water fraction. The PL spectra and relative PL intensities of the host–guest **BP5-H⊃MC-G** and the guest **MC-G** upon the addition of various anions are demonstrated in Fig. 8e and f, respectively. Accordingly, it is worth noting that the PL emission color change from red to green *via* the FRET-OFF process will be advantageous as a novel FRET sensor material due to the ratiometric PL detection of CN^- anion by the bi-fluorophoric host–guest **BP5-H⊃MC-G,** which will be more sensitive than the single red-emission quenching process by the mono-fluorophoric guest **MC-G.**

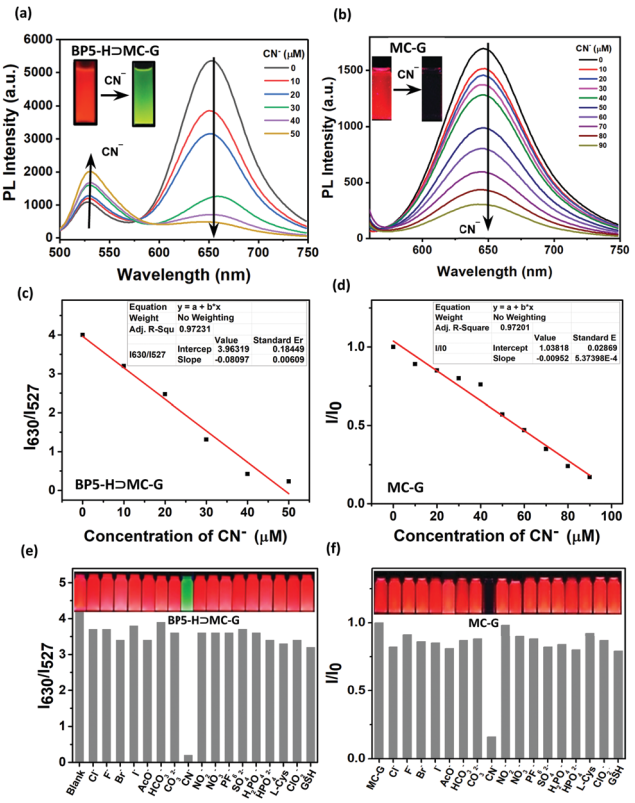

Fig. 8 (a) PL spectra of **BP5-H⊃MC-G** (33 μM) with the increasing concentration of cyanide (0–50 μM). (b) PL spectra of **MC-G** (33 μM) at different concentrations of cyanide ions (0–90 μM). (c) Linear relationship between the PL intensity ratio (I_{630}/I_{527}) of **BP5-H⊃MC-G** (33 μM) and the concentration of cyanide (0–50 μM). (d) Linear relationship between the normalized PL intensity (I/I_0) of **MC-G** (33 μM) and the concentration of cyanide (0–90 μM). (e) PL intensity ratio response of **BP5-H⊃MC-G** (33 μM) upon the addition of various analytes (100 μM). (f) Normalized PL intensity response of **MC-G** (33 μM) with various analytes (100 μM) in THF/water solution (60% H_2O, v/v). Insets: Fluorescence images of **BP5-H⊃MC-G** and **MC-G** in the presence of different analytes after UV exposure. All data were obtained at an excitation wavelength of λ_{ex} = 490 nm.

DLS and TRPL results

To estimate the aggregation sizes of all compounds, the average diameters of all [2]pseudorotaxanes (*i.e.*, **BP5-H**, **SP-G**, **MC-G**, **BP5-H⊃SP-G**, and **BP5-H⊃MC-G**) and the related derivative (*i.e.*, **BP5-H⊃MC-G-CN⁻**) were measured using dynamic light scattering (DLS) experiments, and their sizes are illustrated in Fig. S36 (ESI†) and Table 1. Regardless of the large average size of the host **BP5-H** (d = 458 nm), the average sizes of both guests, **SP-G** (d = 103 nm) and **MC-G** (d = 267 nm), are smaller than those of their corresponding host–guest system in **BP5-H⊃SP-G** (d = 305 nm) and **BP5-H⊃MC-G** (d = 530 nm). With a similar trend of the open form after UV exposure, both the guest **MC-G** (267 nm) and the host–guest **BP5-H⊃MC-G** (530 nm) exhibited average sizes larger than the respective average sizes of the guest **SP-G** (103 nm) and the host–guest **BP5-H⊃SP-G** (305 nm), which could be attributed to the longer conjugated structure of **MC-G** after UV exposure to induce larger aggregations in both the guest and the host–guest systems containing **MC-G.** Moreover, the reacted host–guest **BP5-H⊃MC-G-CN⁻** after cyanide detection showed a smaller average size of 383 nm than that of the host–guest **BP5-H⊃MC-G** (530 nm), which might be because of the reaction of the MC unit with CN^- to reduce the conjugation and aggregation of the host–guest system.

To further investigate the FRET process between the green-emissive BODIPY donor and the red-emissive MC acceptor, the time-resolved photoluminescence (TRPL) spectra and their lifetime values (excited at λ_{ex} = 490 nm, λ_{em} = 523 nm) of the host **BP5-H**, host–guest systems (**BP5-H⊃SP-G** and **BP5-H⊃MC-G**) and the reacted host–guest system (**BP5-H⊃MC-G-CN⁻**) after CN^- ion detection are illustrated in Fig. S37 (ESI†) and Table 1.

Table 1 Average sizes and lifetime values of all compounds in solution[a]

Compound	**BP5-H**	**SP-G**	**MC-G**	**BP5-H⊃SP-G**	**BP5-H⊃MC-G**	**BP5-H⊃MC-G-CN$^-$**
d^b (nm)	458	103	267	305	530	383
τ^c (ns)	3.2	—	—	2.24	0.37	2.50

[a] All compounds measured in THF/water (60% H_2O, v/v) solution (50 μM). [b] Determined using dynamic light scattering (DLS) measurements. [c] Determined using time-resolved photoluminescence (TRPL) measurements at λ_{ex} = 375 nm and λ_{em} = 523 nm.

In contrast, host–guest systems **BP5-H⊃SP-G** and **BP5-H⊃MC-G** have shorter lifetime values of 2.24 and 0.37 ns, respectively, than the host **BP5-H** (3.20 ns) due to the energy transfer between the host and guest components of host–guest systems. Furthermore, the host–guest **BP5-H⊃MC-G** in the open form of MC has a shorter lifetime value of 0.37 ns than the host–guest **BP5-H⊃SP-G** (2.24 ns) in the closed form of SP due to the FRET process from the host (donor) to the guest (acceptor) in the host–guest system. Furthermore, the bi-fluorophoric host–guest **BP5-H⊃MC-G** showed the shortest donor emission lifetime value of 0.37 ns among all TRPL measurements because of the most efficient FRET process. Moreover, the lifetime value (2.50 ns) of the reacted host–guest **BP5-H⊃MC-G-CN$^-$** was much longer than that (0.37 ns) of host–guest **BP5-H⊃MC-G** in Table 1, which confirmed the noticeable FRET-OFF process after the detection of CN^-, and thus to recover the green donor emission of BODIPY unit (**BP5-H**) at λ_{em} = 523 nm. Therefore, the most efficient FRET process along with prominent ratiometric PL emissions between the green BODIPY donor and the red MC acceptor results in the highly potential sensing applications of the bi-fluorophoric host–guest **BP5-H⊃MC-G** toward CN^- ion detection.

Theoretical calculations

As the synthesized photo-switchable supramolecular [2]pseudorotaxane is experimentally investigated, the analyses of energy band structures and the FRET mechanism of the host–guest [2]pseudorotaxane can be carried out *via* theoretical studies. The FRET mechanism allows a fluorophoric donor in an excited electronic state to transfer its energy to another fluorophoric acceptor through long-range dipole–dipole interactions. The proposed mechanism of FRET from the green-emissive BODIPY donor to the red-emissive MC acceptor in the experimental observation of the bi-fluorophoric host–guest **BP5-H⊃MC-G** can be further supported by density functional theory (DFT) calculations. The energy band structures of the photo-switchable [2]pseudorotaxane fluorophore initially and after its reaction with CN^- ions were optimized at the Hartree–Fock (HF) level in the gas phase. Due to the large size of macromolecular structures, it was optimized at the HF level of theory. The single point energy calculations were carried out at the B3LYP/6-31g(d,p) level in the gas phase. Moreover, time-dependent density functional theory (TDDFT) and frontier molecular orbital calculations were carried out at the B3LYP/6-31g(d,p) level using the optimized structure at the HF level of theory. All calculations were performed using the Gaussian09 suite of programs, and the optimized structures of **BP5-H**, **BP5-H⊃MC-G** and **BP5-H⊃MC-G-CN$^-$** are shown in Fig. S38 (ESI†). As shown in Fig. S39 (ESI†), the distance between the phenyl moiety of the BODIPY donor and the indole moiety of the MC acceptor was observed to be 2.1 nm. The required distance (1–10 nm) for the FRET process is satisfied with the distance (2.1 nm) observed in the donor–acceptor moiety as shown in Fig. S39 (ESI†). In **BP5-H⊃MC-G**, three C–H···N hydrogen bonds were observed in the host–guest system, and the bond lengths were noted as 2.738, 2.848 and 2.986 Å as shown in Fig. S38b (ESI†). Two hydrogen bonds of C–H···N and C–H···O were observed in the reacted host–guest system, *i.e.*, **BP5-H⊃MC-G-CN$^-$**, and the hydrogen bond lengths were noted as 2.626 and 2.071 Å, respectively. The electrostatic potential structure of **BP5-H** was obtained at the B3LYP/6-31g(d,p)//HF level of theory in the gas phase. The binding site of **BP5-H** can be observed in the electrostatic potential diagram indicated in red color with a scale of -5.627×10^{-2} to 5.627×10^{2}, as shown in Fig. S40 (ESI†). The frontier molecular orbitals of the host–guest **BP5-H⊃MC-G** and its reacted host–guest **BP5-H⊃MC-G-CN$^-$** are shown in Fig. 9. The electrons of the host–guest **BP5-H⊃MC-G** as shown in Fig. 9a were located on the pillar[5]arene cavity at HOMO−5. When the electrons were shifted to the LUMO, they were migrated to the merocyanine unit. After CN^- detection, the electrons of the reacted host–guest **BP5-H⊃MC-G-CN$^-$** as shown in Fig. 9b were located on the merocyanine unit in the HOMO. When shifted to LUMO+3, it can be observed that the electrons were localized on the BODIPY unit with a bandgap of 1.63 eV. The TDDFT calculations showed a 545 nm absorption, corresponding to the HOMO−5 → LUMO electronic transition. This result is in good agreement with the absorption wavelength of 527 nm observed in experiments. The results of the frontier molecular orbital in the reacted host–guest **BP5-H⊃MC-G-CN$^-$** show a HOMO to LUMO+4 band gap of 1.56 eV with an oscillator strength of f = 0.0017. The TDDFT results show a value of ∼577 nm with respect to the oscillator strength of 0.0017. Hence, the FRET processes of **BP5-H⊃MC-G-CN$^-$** were turned off to quench the red acceptor emission of the guest **MC-G** because the MC unit reacted with CN^- and the green donor emission of the host **BP5-H** recovered partially, which is in accordance with the experimental results shown in Fig. 9b.

Confocal bio-imaging tests

To further investigate the prospect of the host–guest **BP5-H⊃MC-G** with the strongest FRET process as a selective fluorescent sensor for CN^- ion detection, we carried out the confocal fluorescence imaging tests for living cells, in which the cytotoxicity of the closed and open forms of host–guest systems

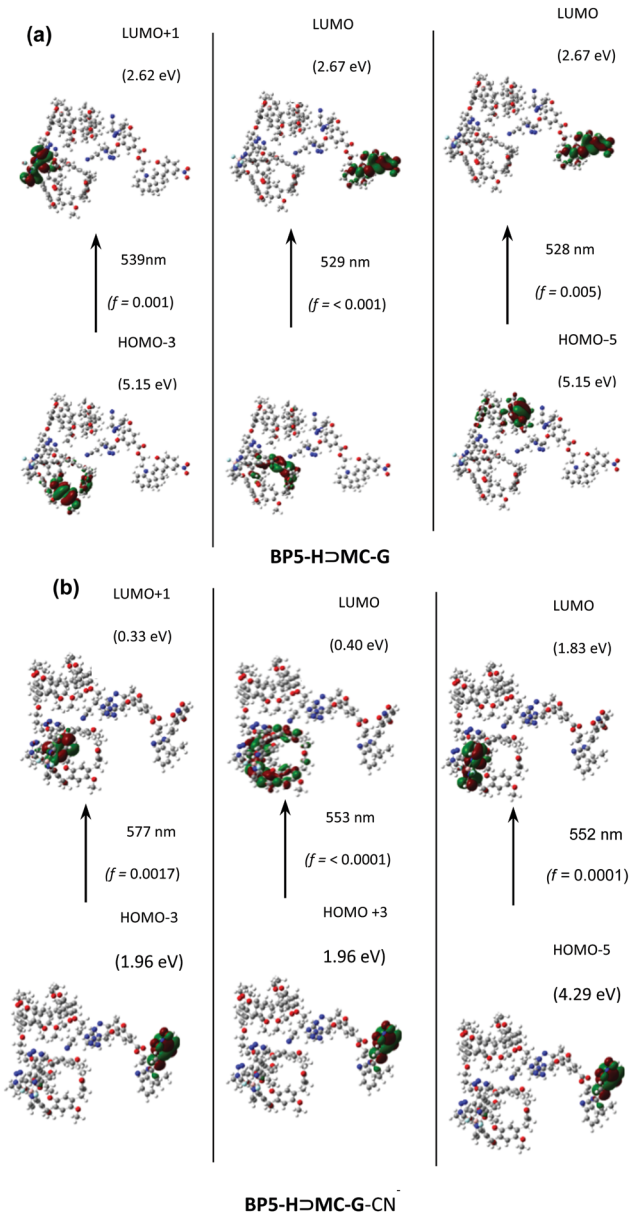

Fig. 9 Electronic transitions and the corresponding molecular orbitals for (a) **BP5-H⊃MC-G** and (b) **BP5-H⊃MC-G-CN**$^-$. Orbital energies were computed at the B3LYP/6-31g(d,p)//HF level in the gas phase.

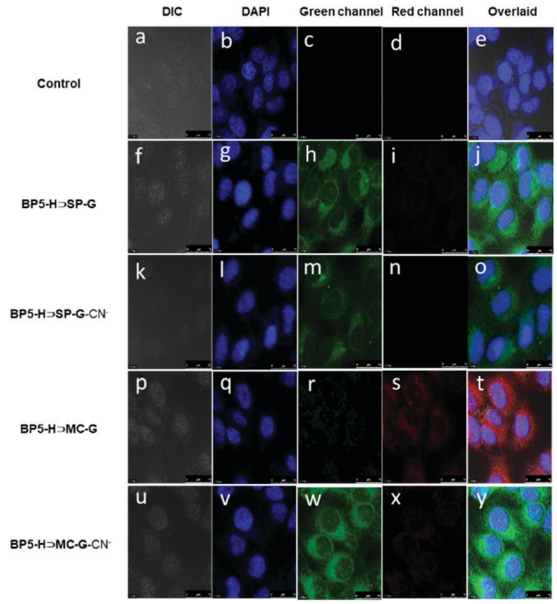

Fig. 10 Confocal fluorescence images of HeLa. (a–e) Control experiments of HeLa. (f–j) Cells were incubated with **BP5-H⊃SP-G** for 30 min. (k–o) Cells were treated with **BP5-H⊃SP-G** for 30 min, followed by incubation with CN^- for 30 min. (p–t) Cells were incubated with **BP5-H⊃MC-G** for 30 min. (u–y) Cells were treated with **BP5-H⊃MC-G**, followed by incubation with CN^- for 30 min. The concentrations of **BP5-H⊃MC-G** and CN^- are 30 μM and 50 μM, respectively. The green and red emissions were collected at 500–550 and 600–650 nm, respectively.

BP5-H⊃SP-G and **BP5-H⊃MC-G** was assessed *via* the standard MTT assay using HeLa cells. Different amounts of host–guest systems, **BP5-H⊃SP-G** and **BP5-H⊃MC-G** (10–50 μM), were added to the preliminary medium and incubated at 37 °C with 5% CO_2 for 24 h. After this, the MTT solution was removed and the yellow precipitates (formazan) were dissolved in μL DMSO and 25 μL Sorensen's glycine buffer (0.1 M glycine and 0.1 M NaCl). As shown in Fig. S41 (ESI†), when the cells were treated with 50 μM host–guest systems for 24 hours, the cell viabilities were 70%, signifying that both the closed and open forms of host–guest systems **BP5-H⊃SP-G** and **BP5-H⊃MC-G** had low cytotoxicity. Due to the FRET process of the bi-fluorophoric host–guest system, **BP5-H⊃MC-G** can be applied to examine the bio-imaging of HeLa cells using confocal fluorescence microscopy. Besides control experiments (see Fig. 10a–e), the related confocal bio-images of host–guest systems **BP5-H⊃SP-G** and **BP5-H⊃MC-G** along with both host–guest systems after CN^- detection are shown in Fig. 10. In general, the host–guest **BP5-H⊃SP-G**, in its closed form, shows an intense green channel PL emission as shown in Fig. 10h. In contrast, the open form of the host–guest **BP5-H⊃MC-G** had a strong red channel PL emission as shown in Fig. 10s, and its green channel PL emission as shown in Fig. 10r was decreased due to the FRET-ON process. As demonstrated in Fig. 10k–o, the closed form of **BP5-H⊃SP-G** did not show any noticeable PL changes after the addition of CN^- ions. In contrast, the open form of **BP5-H⊃MC-G** revealed obvious PL emission color changes from red to green after the addition of CN^- ions as shown in Fig. 10u–y due to the FRET-OFF processes. Based on the above experiments, these results indicate that the open form of the host–guest **BP5-H⊃MC-G** could be utilized for the bio-imaging applications of cyanide detection in living cells.

Conclusions

In summary, we have developed a mono-fluorophoric host–guest, namely, **BP5-H⊃SP-G** (closed form) containing the green-emissive (λ_{em} = 523 nm) BODIPY-based pillar[5]arene host **BP5-H** and the non-emissive SP-based cyano guest **SP-G**, which can be converted to a red-emissive (λ_{em} = 630 nm) guest

MC-G (open form) upon UV exposure as well as turned into the bi-fluorophoric host–guest **BP5-H⊃MC-G** (open form) in semi-aqueous media. The matchable energy transfer between the green-emissive BODIPY donor and the red-emissive MC acceptor induces the FRET process of bi-fluorophoric **BP5-H⊃MC-G**, in which the photochromic MC/SP moieties upon respective UV/visible light exposure can initiate the corresponding FRET ON/OFF processes along with ratiometric PL behavior in this study. The 1 : 1 molar ratio between the host **BP5-H** and the guest **SP-G** and the formation of the [2]pseudorotaxane polymer **BP5-H⊃SP-G** were further verified using ^{1}H NMR titration, Job's plot analysis, DOSY and ITC experiments. Hence, the host–guest **BP5-H⊃MC-G** in the THF/water solution (60% H_2O, v/v) possesses the best FRET process and the highest red-emission of the MC acceptor, which was also verified using TRPL measurements to possess the shortest lifetime of 0.37 ns and the best FRET efficiency of 83.5%. The effects of pH and temperature were studied, and it was found that an efficient FRET process of the host–guest **BP5-H⊃MC-G** could occur at neutral pH values (*i.e.*, pH = 5–9) and temperature in the range of 10–40 °C. The MC unit could react with CN^- to induce the quenching process (*i.e.*, turn-off PL behavior), so a LOD value of 0.94 μM for the mono-fluorophoric guest **MC-G** toward cyanide ions was obtained. In comparison, the best LOD value of 0.48 μM toward CN^- anion was achieved by our bi-fluorophoric host–guest system (*i.e.*, **BP5-H⊃MC-G-CN$^-$**). Accordingly, due to the ratiometric PL detection of CN^- anion by the bi-fluorophoric host–guest **BP5-H⊃MC-G**, it is worth noting that the PL emission color change from red to green *via* the FRET-OFF process will be advantageous as a novel FRET sensor material, which will be more sensitive than a single red-emission quenching process induced by the mono-fluorophoric guest **MC-G**. Furthermore, the LOD values of both **BP5-H⊃MC-G** and **MC-G** are much lower than the maximum permissible limit of cyanide in drinking water (*i.e.*, 1.9 μM (70 ppb) set by the WHO. Hence, the cell viability test experiments suggest that the open form of the host–guest **BP5-H⊃MC-G** could be utilized for cyanide detection in living cells for bio-imaging applications.

Experimental section

Materials and characterization

Chemicals were purchased from commercial sources (Sigma-Aldrich, TCI Japan and J. T. Baker) and directly used as received. All solvents were dried by distillation over appropriate drying agents. All of the anhydrous reactions were carried out under nitrogen atmosphere to avoid moisture. Different anion solutions (Cl^-, F^-, Br^-, I^-, AcO^-, HCO_3^-, CO_3^{2-}, CN^-, NO_2^-, NO_3^-, PF_6^-, SO_4^{2-}, $H_2PO_4^-$, HPO_4^{2-}, L-Cys, ClO_2^- and GSH) were prepared in distilled water from their sodium, potassium and ammonium salts.

Characterization studies and measurements

^{1}H NMR and ^{13}C NMR spectra were measured using a Bruker Avance 300 or a Varian 500 MHz instrument. All chemical shifts (δ) were expressed in parts per million from low to high fields and coupling constants (J) in Hertz. High-resolution mass spectra (HRMS) (ESI,† mode) were recorded using a Bruker-Impact HD mass spectrometer. UV-vis spectra were recorded using a Hitachi U-4100 UV-vis spectrophotometer under different solvent conditions. Fluorescence spectra were conducted using a Hitachi F-7000 spectrophotometer. Dynamic light scattering (DLS) analyses were conducted using an Otsuka Electronics particle Analyzer ELSZ-2000. The isothermal calorimetry (ITC) experiments were carried out using a MicroCal iTC-200 instrument (GE Healthcare) at 298 K. The titrant volume of injection was 20 μL. To correct the thermal effect due to mixing and dilution, control experiments were performed by injecting the titrant into pure water.

Cell culture and confocal fluorescence imaging

The HeLa cells were grown in DMEM (Dulbecco's Modified Eagle Medium) media supplemented with 10% (v/v) FBS (fetal bovine serum) and penicillin/streptomycin (100 μg mL^{-1}) at 37 °C in a 5% CO_2 incubator. The cell culture experiments to evaluate the sensing ability of host–guest systems **BP5-H⊃SP-G** and **BP5-H⊃MC-G** (before and after 10 min of UV irradiation) toward CN^- ions (50 μM) in living cells were performed in 0.1 M phosphate-buffered saline (PBS). The cells were treated with 30 μM of host–guest systems **BP5-H⊃SP-G** and **BP5-H⊃MC-G** incubated for 30 min at 37 °C. After the culture medium was removed, the treated cells were washed with 0.1 M PBS (2 mL × 3) before observation. The confocal fluorescence images of cells were acquired using a Leica TCS SP5 X AOBS Confocal Fluorescence Microscope (Germany), and a 63× oil-immersion objective lens was used. Green and red emissions were collected at 500–550 nm and 600–650 nm, respectively.

Cytotoxicity assay

The cellular cytotoxicity of **BP5-H⊃MC-G** in HeLa cells was evaluated using the methyl thiazolyl tetrazolium (MTT) assay. HeLa cells were grown in a 96-well cell-culture plate and several concentrations (10, 20, 30, 40 and 50 μM) of **BP5-H⊃MC-G** were added to the wells. Then, the cells were incubated at 37 °C under 5% CO_2 for 24 h. Thereafter, each well was incubated with 20 μL MTT (2 mg mL^{-1}) at 37 °C under 5% CO_2 for 4 h. The MTT solution was removed and the yellow precipitates (formazan) were dissolved in 200 μL DMSO and 25 μL Sorensen's glycine buffer (0.1 M glycine and 0.1 M NaCl). The absorbance at 570 nm for each well was measured using the Multiskan GO microplate reader. The viability of the cells was calculated using the following equation:

Cell viability (%) = (mean of absorbance value of treatment group)/(mean of absorbance value of control group).

Synthesis and characterization

The detailed information on the synthesis and characterization of intermediates is given in the ESI† (Schemes S1 and S2). The synthetic procedures of host **BP5-H** and guest **SP-G** are illustrated

in Scheme 1. The boron-dipyrromethene (BODIPY)-bridged pillar[5]arene host (**BP5-H**) was synthesized by facile click reaction between propargyloxy group containing BODIPY (**H-5**) and azide functionalized pillar[5]arene (**H-3**) in the presence of the catalyst $[Cu(CH_3CN)_4]PF_6$ in DCM medium. Likewise, the photoswitchable spiropyran guest **SP-G** containing dicyano units was obtained by click reaction between two key intermediates **G-6** and 3-azidopropanenitrile. The detailed synthetic processes of intermediates **H-3**, **H-5** and **G-6** are described in the ESI,† and they were successfully prepared by following the procedures reported in the literature.[69] The final compounds (**BP5-H** and **SP-G**) along with all intermediates have been fully characterized using ^{1}H and ^{13}C NMR spectroscopy and high-resolution mass spectrometry (HRMS), which are shown in Fig. S1–S20 (ESI†).

Synthesis of host BP5-H

Compound **H3** (354.60 mg, 0.44 mmol) and **H5** (75 mg, 0.20 mmol) were dissolved in DCM (100 mL). Then, $[Cu(MeCN)_4]PF_6$ (163 mg, 0.44 mmol, 2.2 equiv.) was added and the mixture was stirred to react at room temperature for 24 h. Consequently, the mixture was quenched with water (50 mL) and extracted using DCM (3 × 40 mL). The combined organic extracts were dried over anhydrous Na_2SO_4 and concentrated under reduced pressure. The crude product was purified using column chromatography (silica gel, DCM : MeOH = 99 : 1 v/v) to give compound **BP5-H** as an orange-red solid. Yield: 124 mg (30%).

^{1}H NMR (500 MHz, 1 : 1 $CDCl_3$–CD_3CN, 298 K): 7.93 (d, J = 3.5 Hz, 1H), 7.88–7.85 (m, 3H), 7.31 (d, J = 2.5 Hz, 1H), 7.19–7.17 (m, 1H), 7.12–7.10 (m, 1H), 6.94 (d, J = 3.5 Hz, 2H), 6.86–6.79 (m, 16H), 6.67 (dd, J = 6.0, 2.5 Hz, 3H), 6.53 (d, J = 2.0 Hz, 3H), 5.24 (s, 2H), 5.17 (s, 2H), 4.75–4.72 (m, 4H), 4.29–4.26 (m, 4H), 3.72–3.43 (m, 74H). ^{13}C NMR (125 MHz, $CDCl_3$) δ 152.3, 151.7, 151.6, 151.5, 151.4, 149.7, 144.3, 135.4, 132.2, 129.5, 129.4, 129.3, 129.1, 128.8, 128.6, 128.4, 125.8, 125.1, 119.0, 118.1, 115.9, 115.1, 115.0, 114.8, 114.6, 67.7, 63.9, 63.6, 56.8, 56.6, 56.4, 56.3, 50.6, 31.0, 30.7, 30.4, 30.1. HRMS (ESI$^+$) $[M + H]^+$: calcd for $C_{113}H_{118}BF_2N_8O_{22}$ 1988.8458, found 1988.8594. M.p. 138–140.0 °C.

Synthesis of guest SP-G

Compounds 3-azidopropanenitrile (16.9 mg, 0.176 mmol, 2.2 equiv.) and **G-6** (50 mg, 0.08 mmol, 1 equiv.) were dissolved in dry DCM (50 mL). Then, $[Cu(MeCN)_4]PF_6$ (65.5 mg, 0.176 mmol, 2.2 equiv.) was added to the mixture and stirred to react at room temperature for 2 days, and the reaction was monitored using thin-layer chromatography (DCM : MeOH = 99 : 1 v/v). Consequently, the mixture was quenched with water (20 mL) and extracted using DCM (3 × 20 mL). The combined organic extracts were dried over anhydrous Na_2SO_4 and concentrated under reduced pressure. The resultant crude was purified using silica gel column chromatography (DCM : MeOH = 99 : 1 v/v) to give **SP-G** as a purple solid. Yield: 46 mg, (50%). ^{1}H NMR (500 MHz, 1 : 1 $CDCl_3$–CD_3CN, 298 K): 7.97 (d, J = 2.5 Hz, 1H), 7.93 (s, 2H), 7.89 (dd, J_1 = 9 Hz, J_2 = 3 Hz, 1H), 7.16–7.14 (m, 3H), 7.08 (d, J = 7 Hz, 1H), 6.98 (d, J = 10 Hz, 1H), 6.84–6.82 (m, 2H), 6.75 (d, J = 8 Hz, 1H), 6.64 (d, J = 9 Hz, 1H), 5.90 (d, J = 10.5 Hz, 1H), 5.13 (s, 4H), 4.64 (t, J = 6.5 Hz, 4H), 4.41 (t, J = 5 Hz, 2H), 3.64–3.52 (m, 2H), 3.04 (t, J = 6.5 Hz, 4H), 1.23 (s, 3H), 1.10 (s, 3H). ^{13}C NMR (125 MHz, 1 : 1 $CDCl_3$–CD_3CN) δ 166.3, 160.0, 147.4, 141.6, 136.5, 132.7, 123.4, 122.3, 119.4, 116.0, 109.2, 107.3, 64.0, 62.4, 53.4, 46.2, 42.8, 19.6. HRMS (ESI$^+$) $[M + H]^+$: calcd for $C_{39}H_{36}N_{10}O_7$ 757.2856, found 757.2852. M.p. 170–172.0 °C.

Conflicts of interest

There are no conflicts to declare.

Acknowledgements

The authors are grateful for funding from the Ministry of Science and Technology, Taiwan, ROC. This work was supported by the Ministry of Science and Technology, Taiwan (grant no. MOST106-2113-M-009-012-MY3, MOST107-2221-E-009-043-MY2 and MOST108-3017-F-009-004) and the Center for Emergent Functional Matter Science of National Chiao Tung University from The Featured Areas Research Center Program within the framework of the Higher Education Sprout Project by the Ministry of Education (MOE) in Taiwan.

References

1 R. Jackson, R. P. Oda, R. K. Bhandari, S. B. Mahon, M. Brenner, G. A. Rockwood and B. A. Logue, *Anal. Chem.*, 2014, **86**, 1845–1852.
2 R. Koenic, *Science*, 2000, **287**, 1737–1738.
3 F. J. Baud, *Hum. Exp. Toxicol.*, 2007, **26**, 191–201.
4 L. Long, M. Huang, N. Wang, Y. Wu, K. Wang, A. Gong, Z. Zhang and J. L. Sessler, *J. Am. Chem. Soc.*, 2018, **140**, 1870–1875.
5 P. Q. Nhien, W.-L. Chou, T. T. K. Cuc, T. M. Khang, C.-H. Wu, N. Thirumalaivasan, B. T. B. Hue, J. I. Wu, S.-P. Wu and H.-C. Lin, *ACS Appl. Mater. Interfaces*, 2020, **12**, 10959–10972.
6 I. Programme and O. N. Chemical, *Guidelines for drinking-water quality*, Health criteria and other supporting information, 2nd edn, 1996, vol. 2, p. 2.
7 D. T. Thompson, *Gold Bull.*, 2001, **34**, 133–135.
8 K. Keshav, P. Torawane, M. Kumar Kumawat, K. Tayade, S. K. Sahoo, R. Srivastava and A. Kuwar, *Biosens. Bioelectron.*, 2017, **92**, 95–100.
9 F. Wang, L. Wang, X. Chen and J. Yoon, *Chem. Soc. Rev.*, 2014, **43**, 4312–4324.
10 K. Deng, L. Wang, Q. Xia, R. Liu and J. Qu, *Sens. Actuators, B*, 2019, **296**, 126645.
11 R. Kaushik, R. Sakla, A. Ghosh, S. Dama, A. Mittal and D. A. Jose, *ACS Appl. Mater. Interfaces*, 2019, **11**, 47587–47595.
12 Z. Xu, X. Chen, H. N. Kim and J. Yoon, *Chem. Soc. Rev.*, 2010, **39**, 127–137.

13 H. S. Jung, J. H. Han, Z. H. Kim, C. Kang and J. S. Kim, *Org. Lett.*, 2011, **13**, 5056–5059.
14 B. Vidya, M. Iniya, G. Sivaraman, R. V. Sumesh and D. Chellappa, *Sens. Actuators, B*, 2017, **242**, 434–442.
15 Y. Shiraishi, S. Sumiya, K. Manabe and T. Hirai, *ACS Appl. Mater. Interfaces*, 2011, **3**, 4649–4656.
16 X. Lv, J. Liu, Y. Liu, Y. Zhao, M. Chen, P. Wang and W. Guo, *Org. Biomol. Chem.*, 2011, **9**, 4954–4958.
17 R. Merckx, T. Swift, R. Rees, J. F. R. Van Guyse, E. Schoolaert, K. De Clerck, H. Ottevaere, H. Thienpont, V. V. Jerca and R. Hoogenboom, *J. Mater. Chem. C*, 2020, **8**, 14125–14137.
18 J. Zhang, S.-X. Tang, R. Fu, X.-D. Xu and S. Feng, *J. Mater. Chem. C*, 2019, **7**, 13786–13793.
19 P. Wang, S. Guo, H.-J. Wang, K.-K. Chen, N. Zhang, Z.-M. Zhang and T.-B. Lu, *Nat. Commun.*, 2019, **10**, 3155.
20 M. Poddar, G. Sivakumar and R. Misra, *J. Mater. Chem. C*, 2019, **7**, 14798–14815.
21 J. Mei, N. L. C. Leung, R. T. K. Kwok, J. W. Y. Lam and B. Z. Tang, *Chem. Rev.*, 2015, **115**, 11718–11940.
22 Z. Yang, W. Xu, J. Wang, L. Liu, Y. Chu, Y. Wang, Y. Hu, T. Yi and J. Hua, *J. Mater. Chem. C*, 2020, **8**, 8183–8190.
23 J. Zou, P. Wang, Y. Wang, G. Liu, Y. Zhang, Q. Zhang, J. Shao, W. Si, W. Huang and X. Dong, *Chem. Sci.*, 2019, **10**, 268–276.
24 K. C. Dissanayake, P. O. Ebukuyo, Y. J. Dhahir, K. Wheeler and H. He, *Chem. Commun.*, 2019, **55**, 4973–4976.
25 H.-X. Yu, J. Zhi, T. Shen, W. Ding, X. Zhang and J.-L. Wang, *J. Mater. Chem. C*, 2019, **7**, 8888–8897.
26 J. G. S. Moo, S. Presolski and M. Pumera, *ACS Nano*, 2016, **10**, 3543–3552.
27 Z. Tang, W. Wang, Y. Pi, J. Wang, C. Li, R. Tan and D. Yin, *ACS Sustainable Chem. Eng.*, 2019, **7**, 17967–17978.
28 P. Howlader, B. Mondal, P. C. Purba, E. Zangrando and P. S. Mukherjee, *J. Am. Chem. Soc.*, 2018, **140**, 7952–7960.
29 R. Klajn, *Chem. Soc. Rev.*, 2014, **43**, 148–184.
30 W. Szymański, J. M. Beierle, H. A. v. Kistemaker, W. A. Velema and B. L. Feringa, *Chem. Rev.*, 2013, **113**, 6114–6178.
31 A. Julià-López, J. Hernando, D. Ruiz-Molina, P. González-Monje, J. Sedó and C. Roscini, *Angew. Chem., Int. Ed.*, 2016, **55**, 15044–15048.
32 L. Huang, C. Wu, L. Zhang, Z. Ma and X. Jia, *ACS Appl. Mater. Interfaces*, 2018, **10**, 34475–34484.
33 M. H. Barbee, K. Mondal, J. Z. Deng, V. Bharambe, T. V. Neumann, J. J. Adams, N. Boechler, M. D. Dickey and S. L. Craig, *ACS Appl. Mater. Interfaces*, 2018, **10**, 29918–29924.
34 L. Kortekaas, O. Ivashenko, J. T. van Herpt and W. R. Browne, *J. Am. Chem. Soc.*, 2016, **138**, 1301–1312.
35 D. Wang, T. Zhang, B. Wu, C. Ye, Z. Wei, Z. Cao and G. Wang, *Macromolecules*, 2019, **52**, 7130–7136.
36 Y. Shiraishi, M. Nakamura, N. Hayashi and T. Hirai, *Anal. Chem.*, 2016, **88**, 6805–6811.
37 W. Tian, J. Zhang, J. Yu, J. Wu, J. Zhang, J. He and F. Wang, *Adv. Funct. Mater.*, 2018, **28**, 1703548.
38 J. Ji, X. Li, T. Wu and F. Feng, *Chem. Sci.*, 2018, **9**, 5816–5821.
39 A. K. Dwivedi, R. Singh, A. Singh, K. H. Wei, C. Y. Wu, P. C. Lyu and H. C. Lin, *Macromolecules*, 2016, **49**, 5587–5598.
40 I. S. Park, Y.-S. Jung, K.-J. Lee and J.-M. Kim, *Chem. Commun.*, 2010, **46**, 2859–2861.
41 P. Q. Nhien, T. T. K. Cuc, T. M. Khang, C.-H. Wu, B. B. Hue, J. I. Wu, B. W. Mansel, H.-L. Chen and H.-C. Lin, *ACS Appl. Mater. Interfaces*, 2020, **9**, 47921–47938.
42 R. Singh, A. K. Dwivedi, A. Singh, C. M. Lin, R. Arumugaperumal, K. H. Wei and H. C. Lin, *ACS Appl. Mater. Interfaces*, 2016, **8**, 6751–6762.
43 D. Dai, Z. Li, J. Yang, C. Wang, J.-R. Wu, Y. Wang, D. Zhang and Y.-W. Yang, *J. Am. Chem. Soc.*, 2019, **141**, 4756–4763.
44 M. J. Webber, E. A. Appel, E. W. Meijer and R. Langer, *Nat. Mater.*, 2016, **15**, 13–26.
45 X. Li, H. Zhang, P. Zhang and Y. Yu, *Chem. Mater.*, 2018, **30**, 3752–3758.
46 A. Khan, R. R. Kisannagar, C. Gouda, D. Gupta and H.-C. Lin, *J. Mater. Chem. A*, 2020, **8**, 19954–19964.
47 T. Ogoshi, T. Kakuta and T. Yamagishi, *Angew. Chem., Int. Ed.*, 2019, **58**, 2197–2206.
48 A. S. Mahadevi and G. N. Sastry, *Chem. Rev.*, 2016, **116**, 2775–2825.
49 A. Jain and S. J. George, *Mater. Today*, 2015, **18**, 206–214.
50 Y. Zhao, F. Fay, S. Hak, J. Manuel Perez-Aguilar, B. L. Sanchez-Gaytan, B. Goode, R. Duivenvoorden, C. de Lange Davies, A. Bjørkøy, H. Weinstein, Z. A. Fayad, C. Pérez-Medina and W. J. M. Mulder, *Nat. Commun.*, 2016, **7**, 11221.
51 S. Wang, W. Gao, X.-Y. Hu, Y.-Z. Shen and L. Wang, *Chem. Commun.*, 2019, **55**, 4137–4149.
52 C. J. Pedersen, *J. Am. Chem. Soc.*, 1970, **92**, 391–394.
53 P. Dowari, S. Das, B. Pramanik and D. Das, *Chem. Commun.*, 2019, **55**, 14119–14122.
54 G. Cera, M. Bazzoni, A. Arduini and A. Secchi, *Org. Lett.*, 2020, **22**, 3702–3705.
55 T. Ogoshi, T. Yamagishi and Y. Nakamoto, *Chem. Rev.*, 2016, **116**, 7937–8002.
56 J. Wankar, N. G. Kotla, S. Gera, S. Rasala, A. Pandit and Y. A. Rochev, *Adv. Funct. Mater.*, 2020, 1909049.
57 A. Harada, Y. Takashima and M. Nakahata, *Acc. Chem. Res.*, 2014, **47**, 2128–2140.
58 T. Ogoshi, S. Kanai, S. Fujinami, T. Yamagishi and Y. Nakamoto, *J. Am. Chem. Soc.*, 2008, **130**, 5022–5023.
59 W.-B. Hu, W.-J. Hu, Y. A. Liu, J.-S. Li, B. Jiang and K. Wen, *Chem. Commun.*, 2016, **52**, 12130–12142.
60 K. Yang, Y. Pei, J. Wen and Z. Pei, *Chem. Commun.*, 2016, **52**, 9316–9326.
61 C. Schönbeck, H. Li, B.-H. Han and B. W. Laursen, *J. Phys. Chem. B*, 2015, **119**, 6711–6720.
62 H. Zhu, Q. Li, Z. Gao, H. Wang, B. Shi, Y. Wu, L. Shangguan, X. Hong, F. Wang and F. Huang, *Angew. Chem., Int. Ed.*, 2020, **132**, 10960–10964.
63 M. Xue, Y. Yang, X. Chi, X. Yan and F. Huang, *Chem. Rev.*, 2015, **115**, 7398–7501.

64 L. Geng, X. Yu, Y. Li, Y. Wang, Y. Wu, J. Ren, F. Xue and T. Yi, *Nanoscale*, 2019, **11**, 4044–4052.
65 W. Sun, S. Guo, C. Hu, J. Fan and X. Peng, *Chem. Rev.*, 2016, **116**, 7768–7817.
66 J. Zhou, G. Yu, Y. Li, J. Shen, M. Wang, Z. Li, P. Wei, J. Tang and F. Huang, *Chem. – Eur. J.*, 2019, **25**, 14447–14453.
67 L.-L. Tan, Y. Zhang, B. Li, K. Wang, S. X.-A. Zhang, Y. Tao and Y.-W. Yang, *New J. Chem.*, 2014, **38**, 845–851.
68 N. Song, D.-X. Chen, Y.-C. Qiu, X.-Y. Yang, B. Xu, W. Tian and Y.-W. Yang, *Chem. Commun.*, 2014, **50**, 8231–8234.
69 L. B. Meng, D. Li, S. Xiong, X. Y. Hu, L. Wang and G. Li, *Chem. Commun.*, 2015, **51**, 4643–4646.